

Dynamic analysis of FG porous nano-beams using HOSDT and various porosity and volume fraction models

B. REBAI¹⁾, T. MESSAS¹⁾, Z. S. HAFED²⁾, A. M. ZENKOUR^{3,4)}

¹⁾ Faculty of Sciences & Technology, Civil Engineering Department,
University Abbes Laghrour, Khenchela, Algeria,
e-mail: billeg.rebai@univ-khenchela.dz, billegrebai@yahoo.fr

²⁾ Department of Mathematics, Faculty of Science, King Khalid University,
Abha 21589, Saudi Arabia, e-mail: zhafith@kku.edu.sa

³⁾ Department of Mathematics, Faculty of Science, King Abdulaziz University,
P.O. Box 80203, Jeddah 21589, Saudi Arabia,
e-mail: zenkour@kau.edu.sa (corresponding author)

⁴⁾ Department of Mathematics, Faculty of Science, Kafrelsheikh University,
Kafrelsheikh 33516, Egypt, e-mail: zenkour@sci.kfs.edu.eg (corresponding author)

THIS STUDY PRESENTS A COMPREHENSIVE FRAMEWORK for analyzing the free vibration behavior of functionally graded (FG) porous nanobeams. A high-order shear deformation theory is employed to formulate the governing equations of motion, incorporating Eringen's nonlocal differential constitutive relations within the context of a refined three-variable beam theory. The formulation captures small-scale effects through the length scale parameter and accounts for porosity distributions through various models, including uniform, non-uniform, logarithmic non-uniform, and mass-density-based approaches. Additionally, different volume fraction profiles, such as the power-law, Viola–Tornabene four-parameter, and trigonometric models, are considered to accurately represent the material gradation within the nanobeam. A parametric investigation is conducted to elucidate the influence of critical factors, including the nonlocal parameter, the material index, the length-to-thickness ratio, the porosity coefficient, and porosity distribution patterns, on the dynamic response of the nanobeam. The study provides valuable insights into the interplay between small-scale effects, material heterogeneity, and porosity, offering a comprehensive understanding of their collective impact on the vibration characteristics of FG porous nanobeams.

Key words: dynamic behavior, FG nano-beams, Eringen theory, volume fraction models, porosity distributions, length scale parameter.



Copyright © 2025 The Authors.

Published by IPPT PAN. This is an open access article under the Creative Commons Attribution License CC BY 4.0 (<https://creativecommons.org/licenses/by/4.0/>).

Nomenclature and symbols

Symbol	Description	Unit/Type
Geometric Parameters		
L	Length of the nanobeam	m
b	Width of the nanobeam	m
h	Thickness of the nanobeam	m

Symbol	Description	Unit/Type
Geometric Parameters		
z	Spatial coordinate through thickness	m
x	Spatial coordinate along the length	m
Material Properties		
$P(z)$	Effective material property	Variable
P_c	Property of ceramic phase	Variable
P_m	Property of metal phase	Variable
$V(z)$	Volume fraction of ceramic phase	Dimensionless
p	Material index (power-law exponent)	Dimensionless
$E(z)$	Young's modulus distribution	GPa
E_c	Young's modulus of ceramic	GPa
E_m	Young's modulus of metal	GPa
$\rho(z)$	Mass density distribution	kg/m ³
ρ_c	Mass density of ceramic	kg/m ³
ρ_m	Mass density of metal	kg/m ³
ξ	Porous coefficient	Dimensionless
G	Shear modulus	GPa
Displacement and strain components		
$u(x, z, t)$	Axial displacement	m
$w(x, z, t)$	Transverse displacement	m
$u_0(x, t)$	Mid-plane axial displacement	m
$w_b(x, t)$	Bending component of transverse displacement	m
$w_s(x, t)$	Shear component of transverse displacement	m
ε_x	Normal strain	Dimensionless
γ_{xz}	Shear strain	Dimensionless
ε_x^0	Mid-plane normal strain	Dimensionless
k_x^b	Bending curvature	m ⁻¹
k_x^s	Shear curvature	m ⁻¹
γ_{xz}^s	Shear strain measure	Dimensionless
Stress and force resultants		
σ_x	Normal stress	N/m ²
τ_{xz}	Shear stress	N/m ²
N	Axial force resultant	N
M_b	Bending moment	N · m
M_s	Shear moment	N · m
Q	Shear force	N
Material constants and parameters		
e_0	Material constant	Dimensionless
a	Internal characteristic length	m
μ	Nonlocal parameter, $(e_0 a)^2$	m ²
$f(z)$	Shape function for displacement field	Dimensionless
$g(z)$	Shape function for shear strain	Dimensionless

Symbol	Description	Unit/Type
Mass inertias and stiffness coefficients		
I_0, I_2	Mass inertias	$\text{kg} \cdot \text{m}, \text{kg} \cdot \text{m}^3$
A, B, D	Stiffness coefficients	$\text{N}/\text{m}^2, \text{N}/\text{m}, \text{N}$
B_s, D_s, H_s	Additional stiffness coefficients	$\text{N}/\text{m}, \text{N}, \text{N} \cdot \text{m}$
A_{55}, D_{55}, F_{55}	Shear stiffness coefficients	$\text{N}/\text{m}^2, \text{N}, \text{N} \cdot \text{m}^2$
Dynamic analysis parameters		
ω	Natural frequency	rad/s
$\bar{\omega}$	Non-dimensional frequency	Dimensionless
m	Mode number	Integer
Model-specific parameters		
a, b, c	Viola–Tornabene model parameters	Dimensionless
m_0	Mass at non-zero porosity	kg
m	Mass at zero porosity	kg

1. Introduction

RECENT RESEARCH HAS FOCUSED ON UNDERSTANDING the dynamic behavior of porous functionally graded materials (FGMs) in various structural components. This research highlights the crucial role of porosity, material gradation, nonlocal effects, thermal gradients, and dynamic loading conditions in accurately predicting the dynamic response of these materials.

Studies have demonstrated the significant impact of porosity on the dynamic behavior of FGM structures. RAI and GUPTA [1] investigated the free vibration of FG nanoplates resting on the Winkler–Pasternak elastic foundation, highlighting the influence of porosity on natural frequencies. XIAO *et al.* [2] explored the vibration analysis of porous FG truncated conical shells in axial motion, showcasing the effect of porosity distribution. PHUONG *et al.* [3] examined the nonlinear dynamic buckling of FG-GPLRC panels with a porous core, underlining the role of porosity in buckling behavior. VAKA *et al.* [4] studied the dynamic analysis of a porous exponentially graded shaft system subjected to thermal gradients, showcasing the influence of porosity.

The continuous variation of material properties, or material gradation, within FGM structures also significantly affects their dynamic response. RAI and GUPTA [1] developed a dynamic stiffness matrix to analyze the free vibration of FG-nP, highlighting the influence of material gradation. XIAO *et al.* [2] and PHUONG *et al.* [3] demonstrated the effect of the material composition index on the natural frequencies and buckling behavior of porous FG shells and panels, respectively. VAKA *et al.* [4], CHANDEL and TALHA [5], KURPA *et al.* [6], and ZHANG *et al.* [7] also showcased the influence of material gradation on the dynamic response, stochastic behavior, natural frequencies, and stability of various porous FGM structures.

To account for size-dependent effects in nanoscale structures, researchers have employed nonlocal elasticity theory, which is critical for predicting the dynamic behavior of FGM nanoplates and nanobeams. RAI and GUPTA [1], CHANDEL and TALHA [5], and ZHANG *et al.* [7] highlighted the importance of considering nonlocal effects when analyzing the vibration, stochastic behavior, and stability of porous FG nanostructures.

Researchers have explored the dynamic response of FGM structures subjected to moving loads, harmonic excitations, or impact loading. ZANJANCHI NIKOO *et al.* [8] examined the dynamic instability of Timoshenko FG sandwich nanobeams under parametric excitation. ATTIA and SHANAB [9] analyzed the vibration of 2D-FGM porous nanobeams under a moving load, considering surface stress and microstructure effects. ZANJANCHI *et al.* [10] investigated the dynamic stability and bifurcation point analysis of FG porous core sandwich plates reinforced with graphene platelets. LI and YAN [11] explored the application of a semi-analytical method to the dynamic analysis of FG porous conical-conical-cylindrical shells. In line with this research, AKHZARY and KHORSHIDVAND [12] proposed the mixed differential quadrature-Newmark method to analyze the dynamic response of FGP rectangular plates subjected to moving loads while resting on Winkler-Pasternak elastic foundations. Their study examined the effects of material gradation, porosity distribution, and foundation stiffness on the plate's displacement and stress responses.

Various research approaches have been employed. GIANG *et al.* [13] developed a novel finite element model for the transient analysis of viscoelastic FGP nanoplates resting on the viscoelastic Pasternak medium. By incorporating the higher-order shear deformation theory, nonlocal elasticity, and a refined inverse hyperbolic function, their model effectively captured the influence of porosity, viscoelastic foundation properties, and dynamic loading conditions on the structural response. The Galerkin method [14], the finite element method [15], the generalized differential quadrature method [16], and the Rayleigh-Ritz method [17] are also used.

Recent research has extensively explored the behavior of FGMs in various applications. The static deflection behavior of sandwich FG plates under thermal loads has been a focus, with BILLEL [18] investigating the influence of homogenization models and thermal loads, utilizing micromechanical models to derive effective material properties and validate the analytical model against existing literature. Similarly, REBAI *et al.* [19] examined the deflection of FG plates, evaluating different idealization models to understand their impact on mechanical responses, thus aiding in the efficient design of FGM structures. Moreover, SHEN *et al.* [20] conducted a free vibration analysis of FG porous spherical caps reinforced by graphene platelets on Winkler foundations, highlighting the effect of various parameters, including porosity distribution and graphene platelet

patterns, on the natural frequencies. UZUN *et al.* [21] investigated the torsional dynamic response of FG nanorods using the strain gradient nonlocal elasticity theory, revealing the influence of nonlocal parameters and elastic boundary conditions. Additionally, MADENCI *et al.* [22] explored the free vibration behavior of carbon nanotube-reinforced composite beams using both variational dynamic analysis of FG porous nano-beams analytical methods and artificial neural networks, demonstrating the model's predictive accuracy. TANG and QING [23] focused on the static bending of axially FG nanobeams using local/nonlocal integral models, providing insights into the effects of nonlocal parameters on bending deflections.

In this context, ZARE *et al.* [24] investigated the nonlinear free vibration of bi-directional functionally graded (BFG) Timoshenko nanobeams using the nonlocal elasticity theory and von Kármán nonlinearity. Their study employed the differential quadrature method to discretize the governing equations and analyzed the effects of material gradation, nanobeam length, and nonlocal parameters on the nonlinear frequency response. Similarly, GHANDOURAH *et al.* [25] introduced a novel tri-coated FG shell model to study the free vibration of porous nanoshells resting on a viscoelastic Winkler–Pasternak foundation. Using an analytical Galerkin-based approach, they examined the impact of porosity distribution, material gradient, and nanoshell geometry on the fundamental frequencies, demonstrating the effectiveness of their proposed model across various boundary conditions.

While Eringen's nonlocal elasticity theory has been extensively utilized to model size-dependent effects in nanostructures, it has certain limitations, particularly when applied to bounded structures. Recently, paradoxical results in the characterization of nanobeam responses, primarily due to the assumption that nonlocal effects are uniformly distributed across the structure, which may not be valid for complex boundary conditions have been pointed out [26–34]. However, in the case of FGP nanobeams, Eringen's model remains a practical choice due to its simplicity and its ability to capture the fundamental size-dependent behavior with reasonable accuracy. Although alternative approaches, such as the strain gradient theory and intrinsically nonlocal models [35], offer improved accuracy in certain scenarios, they are computationally intensive. Given the scope of this study, Eringen's nonlocal model provides an optimal balance between computational efficiency and physical reliability for analyzing the mechanical behavior of FG porous nanobeams.

Deep Neural Networks (DNNs) have emerged as a powerful tool for solving Partial Differential Equations (PDEs) in computational mechanics. Traditional methods like the Finite Element Method (FEM) and the Isogeometric Analysis (IGA) rely on discretization, while DNNs offer an alternative by leveraging their function approximation capabilities. Recent approaches, such as the Deep

Autoencoder-based Energy Method (DAEM), integrate machine learning with energy principles to analyze the bending, vibration, and buckling of structures. These methods minimize total potential energy, improving computational efficiency and adaptability. This study explores the application of such techniques to enhance accuracy and efficiency in engineering simulations [36, 37].

This study proposes a unified theoretical framework for dynamic analysis of FG porous nanobeams that integrates the high-order shear deformation theory, Eringen's nonlocal elasticity for capturing small-scale effects, and advanced material modeling techniques. It incorporates various volume fraction models such as the power-law, Viola–Tornabene four-parameter, and trigonometric to represent material gradation, as well as different porosity distributions including uniform, non-uniform, logarithmic non-uniform, and mass-density based patterns. Analytical solutions for natural frequencies of simply supported FG porous nanobeams are derived. Comprehensive parametric investigations elucidate the influence of the length-to-thickness ratio, the nonlocal parameter, the material index, the porosity coefficient, and distribution patterns on vibration characteristics. The framework enables accurate predictions accounting for complexities from small scales, material heterogeneity, and porosity, with implications for optimizing the design of nanobeams in NEMS, energy harvesting, and biomedical sensors, while laying the foundation for future research integrating additional phenomena.

2. Geometric configuration of nanobeams with various applied models

Figure 1 shows a functionally graded (FG) nanobeam of length L , width b , and thickness h . The material on the top surface ($z = +h/2$) of the beam is ceramic and is graded to metal at the bottom surface of the beam ($z = -h/2$).

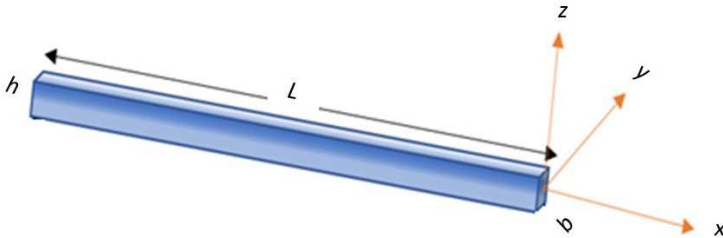


FIG. 1. The geometry domain of the FG nano-beam.

2.1. Mixture law (Voigt model)

The mixture law, also known as the Voigt model, provides a mathematical framework for describing the behavior of composite materials. It postulates that

the properties of a composite material can be derived by linearly combining the properties of its components. This model is instrumental in calculating the effective modulus of elasticity, strength, and other relevant properties of composite materials. The effective material property $P(z)$ is given by:

$$(2.1) \quad P(z) = P_c V(z) + P_m (1 - V(z)),$$

where $P(z)$ is the effective material property. P_m and P_c are the properties of the metal and ceramic faces of the beam, respectively. $V(z)$ denotes the volume fraction of the ceramic phase as a function of the spatial coordinate z . Below there are the models used to describe the volume fraction distributions in FG structures.

2.2. Power-law model

The power-law model defines the volume fraction $V(z)$ as:

$$(2.2) \quad V(z) = \left(\frac{1}{2} + \frac{z}{h} \right)^p,$$

where p is the material index, which influences the gradation profile of the material properties across the beam's thickness.

2.3. Trigonometric model

The trigonometric model expresses the volume fraction $V(z)$ as:

$$(2.3) \quad V(z) = \sin^2 \left(\frac{1}{2} + \frac{z}{h} \right)^p.$$

This model incorporates trigonometric functions to describe the material distribution, offering a different gradation pattern compared to the power-law model.

2.4. Viola–Tornabene four-parameter model

The Viola–Tornabene model introduces a more complex formulation for the volume fraction $V(z)$:

$$(2.4) \quad V(z) = \left[1 - a \left(\frac{1}{2} - \frac{z}{h} \right) + b \left(\frac{1}{2} + \frac{z}{h} \right)^c \right]^p.$$

In this model, a , b , and c are constant parameters that control the material gradation profile within the FG structure. The parameter p further modulates the distribution, allowing for a highly customizable material property variation.

These models collectively enable a comprehensive understanding and precise calculation of the dynamic response of FG porous nano-beams by accounting for

the complex interplay of material distributions and their effects on the beam's behavior.

The porosity varies through the thickness, and four different patterns of porosity variations are examined.

2.5. Even porosities model

The formulations of Young's modulus $E(z)$, mass density $\rho(z)$, can be expressed as follows:

$$(2.5) \quad E(z) = (E_c - E_m) \left(\frac{1}{2} + \frac{z}{h} \right)^p + E_m - \frac{\xi}{2} (E_c + E_m),$$

$$(2.6) \quad \rho(z) = (\rho_c - \rho_m) \left(\frac{1}{2} + \frac{z}{h} \right)^p + \rho_m - \frac{\xi}{2} (\rho_c + \rho_m).$$

2.6. Uneven porosities model

The effective material properties with uneven distribution can be written as:

$$(2.7) \quad E(z) = (E_c - E_m) \left(\frac{1}{2} + \frac{z}{h} \right)^p + E_m - \frac{\xi}{2} (E_c + E_m) \left(1 - \frac{2|z|}{h} \right),$$

$$(2.8) \quad \rho(z) = (\rho_c - \rho_m) \left(\frac{1}{2} + \frac{z}{h} \right)^p + \rho_m - \frac{\xi}{2} (\rho_c + \rho_m) \left(1 - \frac{2|z|}{h} \right).$$

2.7. Logarithmic-uneven porosities

The effective material properties with logarithmic-uneven distribution can be given as:

$$(2.9) \quad E(z) = (E_c - E_m) \left(\frac{1}{2} + \frac{z}{h} \right)^p + E_m - \log \left(1 + \frac{\xi}{2} \right) (E_c + E_m) \left(1 - \frac{2|z|}{h} \right),$$

$$(2.10) \quad \rho(z) = (\rho_c - \rho_m) \left(\frac{1}{2} + \frac{z}{h} \right)^p + \rho_m - \log \left(1 + \frac{\xi}{2} \right) (\rho_c + \rho_m) \left(1 - \frac{2|z|}{h} \right).$$

2.8. Mass-density porosities

The mass-density porosities model is based on the true and the apparent mass density respectively:

$$(2.11) \quad m = \int_h \rho(z) dz \quad \text{at } \xi = 0,$$

$$(2.12) \quad m_0 = \int_h \rho(z) dz \quad \text{at } \xi \neq 0,$$

where ξ is the porous coefficient. The effective material properties with mass-density porosities can be given as:

$$(2.13) \quad E(z) = (E_c - E_m) \left(\frac{1}{2} + \frac{z}{h} \right)^p + E_m - \frac{m_0 - m}{m_0} (E_c + E_m),$$

$$(2.14) \quad \rho(z) = (\rho_c - \rho_m) \left(\frac{1}{2} + \frac{z}{h} \right)^p + \rho_m - \frac{m_0 - m}{m_0} (\rho_c + \rho_m).$$

3. Kinematics

The displacement field in our proposed theory derives from the premise that in-plane and transverse displacements segregate into bending and shear components. The bending aspect of in-plane displacement aligns with the principles of the Euler–Bernoulli theory, while the shear component triggers hyperbolic variations in shear strains and stresses within the plane. Notably, these shear effects diminish at the top and bottom surfaces of the beam. This formulation yields the subsequent displacement field:

$$(3.1) \quad u(x, z, t) = u_0(x, t) - z \frac{\partial w_b}{\partial x} + f(z) \frac{\partial w_s}{\partial x},$$

$$(3.2) \quad w(x, z, t) = w_b(x, t) + w_s(x, t).$$

Here $u_0(x, t)$ denotes the displacements along the x coordinate directions of a point on the mid-plane of the beam; $w_b(x, t)$ and $w_s(x, t)$ are the bending and shear components of the transverse displacements, respectively; and h is the beam thickness. The nonzero strains associated with the displacement field are:

$$(3.3) \quad \varepsilon_x = \varepsilon_x^0 + z k_x^b + f(z) k_x^s, \quad \gamma_{xz} = g(z) \gamma_{xz}^s,$$

where

$$\varepsilon_x^0 = \frac{\partial u_0}{\partial x}, \quad k_x^b = -\frac{\partial^2 w_b}{\partial x^2}, \quad k_x^s = -\frac{\partial^2 w_s}{\partial x^2}, \quad \gamma_{xz}^s = \frac{\partial w_s}{\partial x},$$

$$f(z) = -\frac{1}{4}z + \frac{5}{3}z \left(\frac{z}{h} \right)^2, \quad g = \frac{5}{4} - 5 \left(\frac{z}{h} \right)^2.$$

4. Constitutive relations

The nonlocal constitutive relation for the macroscopic stress tapes the following special relations of Eringen:

$$(4.1) \quad \sigma_x - \mu \frac{d^2 \sigma_x}{dx^2} = E \varepsilon_x, \quad \tau_{xz} - \mu \frac{d^2 \tau_{xz}}{dx^2} = G \gamma_{xz},$$

where E and G are Young's modulus and shear modulus, respectively. Moreover, e_0 is a material constant, and a is the internal characteristic length. Once the nonlocal parameter $\mu = (e_0a)^2$ is equal to zero, we obtain the constitutive relations of the local theories.

Eringen's nonlocal model predicts a "smaller is softer" behavior, contrasting with the "smaller is stiffer" effect observed experimentally. However, in FG porous nanobeams, this prediction aligns with the softening effect caused by porosity and material gradation, leading to lower stiffness and natural frequencies. While the strain gradient theory offers an alternative, it requires complex formulations. Given its simplicity and computational efficiency, Eringen's model remains a practical choice for this study, with the potential for future refinements using advanced models. It assumes linear elasticity, small deformations, and homogeneous porosity distribution. While Eringen's nonlocal theory effectively captures scale effects, it may not fully address size-dependent behavior in bounded structures. Eringen's model has been chosen for its simplicity and applicability to nanostructures but acknowledges alternatives like the strain gradient theory and intrinsically nonlocal methods [38, 39].

5. Equations of motion

Hamilton's principle is used herein to derive the equations of motion. We have obtained:

$$(5.1) \quad \int_0^L \int_A (\sigma_x \delta \varepsilon_x + \tau_{zx} \delta \gamma_{zx}) \, dA \, dx - \int_0^L \int_A \rho [\ddot{u}_0 \delta u_0 + (\ddot{w}_b + \ddot{w}_s) \delta (w_b + w_s)] \, dA \, dx = 0.$$

Integrating by parts Eq. (5.1), and collecting the coefficients of δu_0 , δw_b and δw_s the following equations of stability are obtained:

$$(5.2) \quad \delta u_0: \frac{dN}{dx} = I_0 \ddot{u}_0,$$

$$(5.3) \quad \delta w_b: \frac{d^2 M_b}{dx^2} = I_0 (\ddot{w}_b + \ddot{w}_s) - I_2 \frac{d^2 \ddot{w}_b}{dx^2},$$

$$(5.4) \quad \delta w_s: \frac{d^2 M_s}{dx^2} + \frac{dQ}{dx} = I_0 (\ddot{w}_b + \ddot{w}_s) - \frac{I_2}{84} \frac{d^2 \ddot{w}_s}{dx^2},$$

where N , M_b , M_s and Q are stress resultants and they are defined by:

$$(5.5) \quad (N, M_b, M_s) = \int_A (1, z, f) \sigma_x \, dA, \quad Q = \int_A g \tau_{xz} \, dA$$

and (I_0, I_2) are mass inertias defined as:

$$(5.6) \quad (I_0, I_2) = \int_A (1, z^2) \rho(z) \, dA.$$

Substituting Eqs. (5.2)–(5.4) into Eq. (5.5) and integrating through the thickness of the beam, the stress resultants are related to the generalized displacements by the relations:

$$(5.7) \quad N - \mu \frac{d^2 N}{dx^2} = A \frac{du_0}{dx} - B \frac{d^2 w_b}{dx^2} - B_s \frac{d^2 w_s}{dx^2},$$

$$(5.8) \quad M_b - \mu \frac{d^2 M_b}{dx^2} = B \frac{du_0}{dx} - D \frac{d^2 w_b}{dx^2} - D_s \frac{d^2 w_s}{dx^2},$$

$$(5.9) \quad M_s - \mu \frac{d^2 M_s}{dx^2} = B \frac{du_0}{dx} - D \frac{d^2 w_b}{dx^2} - H_s \frac{d^2 w_s}{dx^2},$$

$$(5.10) \quad Q - \mu \frac{d^2 Q}{dx^2} = A_s \frac{dw_s}{dx},$$

where

$$\{A, B, D, \bar{E}, F, H\} = \int_A \{1, z, z^2, z^3, z^4, z^6\} E(z) \, dA,$$

$$B_s = -\frac{1}{4}B + \frac{5}{3h^2}\bar{E}, \quad D_s = -\frac{1}{4}D + \frac{5}{3h^2}F, \quad H_s = \frac{1}{16}D - \frac{5}{6h^2}F + \frac{25}{9h^4}H,$$

$$\{A_{55}, D_{55}, F_{55}\} = \int_A \{1, z^2, z^4\} G(z) \, dA, \quad A_s = \frac{25}{16}A_{55} - \frac{25}{2h^2}D_{55} + \frac{25}{h^4}F_{55}.$$

After substituting equations, we obtain the following equation in terms of (u_0, w_b, w_s) :

$$(5.11) \quad A \frac{d^2 u_0}{dx^2} - B \frac{d^3 w_b}{dx^3} - B_s \frac{d^3 w_s}{dx^3} = I_0 \left(\ddot{u}_0 - \mu \frac{d^2 \ddot{u}_0}{dx^2} \right),$$

$$(5.12) \quad B \frac{d^3 u_0}{dx^3} - D \frac{d^4 w_b}{dx^4} - D_s \frac{d^4 w_s}{dx^4} \\ = I_0 \left(\ddot{w}_b + \ddot{w}_s - \mu \frac{d^2 (\ddot{w}_b + \ddot{w}_s)}{dx^2} \right) - I_2 \left(\frac{d^2 \ddot{w}_b}{dx^2} - \mu \frac{d^4 \ddot{w}_b}{dx^4} \right),$$

$$(5.13) \quad B_s \frac{d^3 u_0}{dx^3} - D_s \frac{d^4 w_b}{dx^4} - H_s \frac{d^4 w_s}{dx^4} + A_s \frac{d^2 w_s}{dx^2} \\ = I_0 \left(\ddot{w}_b + \ddot{w}_s - \mu \frac{d^2 (\ddot{w}_b + \ddot{w}_s)}{dx^2} \right) - \frac{I_2}{84} \left(\frac{d^2 \ddot{w}_b}{dx^2} - \mu \frac{d^4 \ddot{w}_b}{dx^4} \right).$$

6. Exact solution for a simply-supported FG beam

Following the Navier solution procedure, we assume the solution form for u_0 , w_b , w_s that satisfies a simply-supported FG condition.

$$(6.1) \quad \begin{Bmatrix} u_0 \\ w_b \\ w_s \end{Bmatrix} = \sum_{m=1}^{\infty} \begin{Bmatrix} U_n \cos(\alpha x) \\ W_{bn} \sin(\alpha x) \\ W_{sn} \sin(\alpha x) \end{Bmatrix} e^{i\omega t},$$

where U_n , W_{bn} and W_{sn} are arbitrary parameters to be determined, ω is the eigenfrequency associated with $(n)^{th}$ eigenmode, and the analytical solutions can be obtained from:

$$(6.2) \quad \left(\begin{bmatrix} A\alpha^2 & -B\alpha^3 & -B_s\alpha^3 \\ -B\alpha^3 & D\alpha^4 & D_s\alpha^4 \\ -B_s\alpha^3 & D_s\alpha^4 & H_s\alpha^4 + A_s\alpha^2 \end{bmatrix} - (1 + \mu\alpha^2)\omega^2 \begin{bmatrix} I_0 & -I_1\alpha & -J_1\alpha \\ -I_1\alpha & I_0 + I_2\alpha^2 & I_0 + J_2\alpha^2 \\ -J_1\alpha & I_0 + J_2\alpha^2 & I_0 + K_2\alpha^2 \end{bmatrix} \right) \begin{Bmatrix} U_n \\ W_{bn} \\ W_{sn} \end{Bmatrix} = \begin{Bmatrix} 0 \\ 0 \\ 0 \end{Bmatrix}.$$

7. Parametric study on the natural frequency of the FG porous nanobeams

This section presents a comprehensive parametric study that examines the influence of multiple factors on the natural frequency of FG nanobeams. The analysis investigates the effects of the nonlocal parameter, material index, length-to-thickness ratio, porosity models, and volume fraction distributions. Through a series of figures and numerical results, the study elucidates how these parameters impact the dynamic behavior and natural frequencies of FGM nanobeams composed of aluminum and alumina phases. This systematic analysis aims to enhance the understanding of the dynamics of FG nanobeams, thereby facilitating the design and optimization of these structures for potential applications across various fields.

The FGM nano-beams are composed of aluminum (Al) and alumina (Al_2O_3) phases, representing the metallic and ceramic constituents, respectively.

TABLE 1. Material properties of metal and ceramic.

Material	Young's modulus [GPa]	Mass density [kg/m ³]	Poisson's ratio
Aluminum	70	2702	0.3
Alumina (Al_2O_3)	380	3800	0.3

In all cases, we present the non-dimensional frequency defined as:

$$(7.1) \quad \bar{\omega} = \omega L^2 \sqrt{\frac{\rho_c A}{E_c I}}$$

7.1. Impact of the length-to-thickness ratio on the natural frequency of the FG porous nanobeam

Figure 2 presents a detailed investigation into how the natural frequency of FGM porous nano-beams is influenced by the length-to-thickness ratio (L/h),

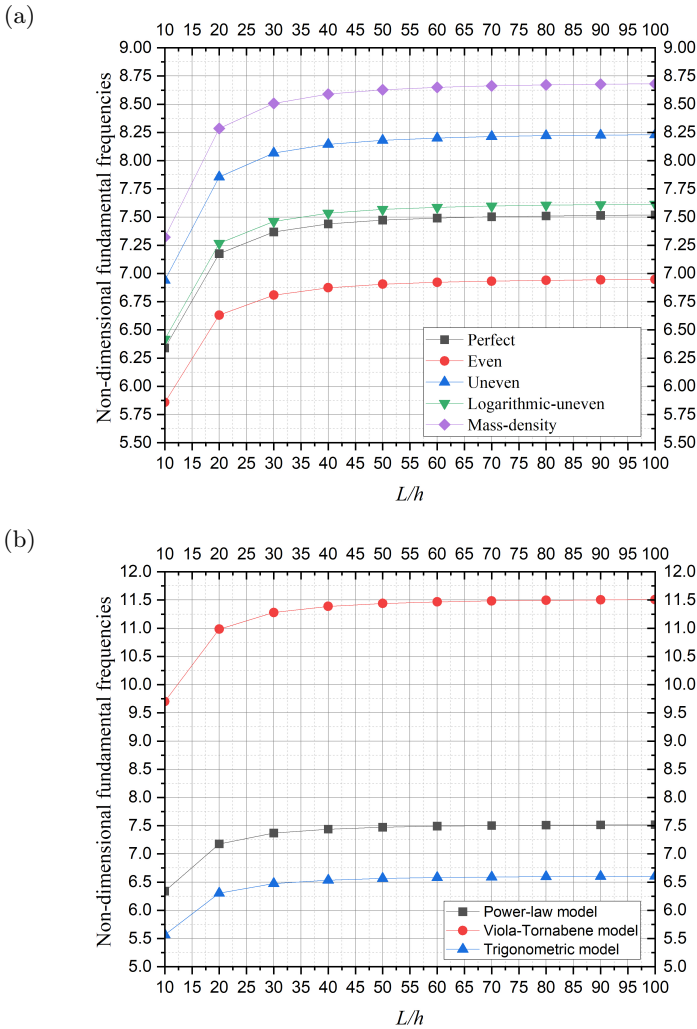


FIG. 2. Natural frequency variation of FG porous nanobeam across different length-to-thickness ratios ($P = 1, \mu = 4$).

across various porosity and volume fraction models. These models include uniform, non-uniform, logarithmic non-uniform, and mass-density-based distributions, as depicted in Fig. 2a. Additionally, the study explores different volume fraction models namely, the power-law, Viola–Tornabene four-parameter, and trigonometric models as illustrated in Fig. 2b. Throughout the analysis, the material index remains constant at 1, while the nonlocal parameter is set to 4.

The trends observed in Fig. 2 indicate that the natural frequency of FG nanobeams tends to increase as the length-to-thickness ratio (L/h) rises. This phenomenon can be understood by considering the structural changes associated with altering the L/h ratio. As the beam becomes longer and thinner, it exhibits higher stiffness and reduced flexibility, leading to an increase in its natural frequency of vibration.

Upon closer examination of the various porosity models, it is apparent that different distributions yield distinct natural frequency responses. Mass-density porosity consistently results in the highest non-dimensional fundamental frequency values, suggesting that a denser material configuration enhances the beam's stiffness and consequently its natural frequency. Conversely, even porosity consistently yields the lowest natural frequency estimates, indicating that a uniform distribution of pores leads to reduced stiffness and lower natural frequencies (Fig. 2a).

Furthermore, the impact of the thickness-to-span ratio (a/h) on the natural frequency is significant. Initially, as the thickness-to-span ratio rises from 10 to 30, there is a rapid escalation in the non-dimensional fundamental frequencies. This acceleration can be ascribed to the heightened stiffness of thicker plates, which resist bending deformations more effectively, resulting in elevated natural frequencies. However, beyond a thickness-to-span ratio of 40, the increase in natural frequency becomes more gradual, suggesting diminishing returns in stiffness enhancement. This observation is visually represented in Fig. 2a.

Regarding the volume fraction models, the Viola–Tornabene four-parameter profile consistently yields the highest values for non-dimensional fundamental frequencies (ω), followed by the power-law model. The trigonometric model, on the other hand, exhibits the lowest deflection, indicating that it leads to a less stiff material configuration compared to the other models (Fig. 2b).

7.2. Effect of nonlocal parameter on the natural frequency of FG nanobeams

Figure 3 presents an exhaustive examination of how the natural frequency of FG porous nano-beams is impacted by the nonlocal parameter, ranging from 0 to 5, across various porosity and volume fraction models. These models encompass diverse distributions, including uniform, non-uniform, logarithmic non-uniform, and mass-density-based distributions, as depicted in Fig. 3a. Additionally,

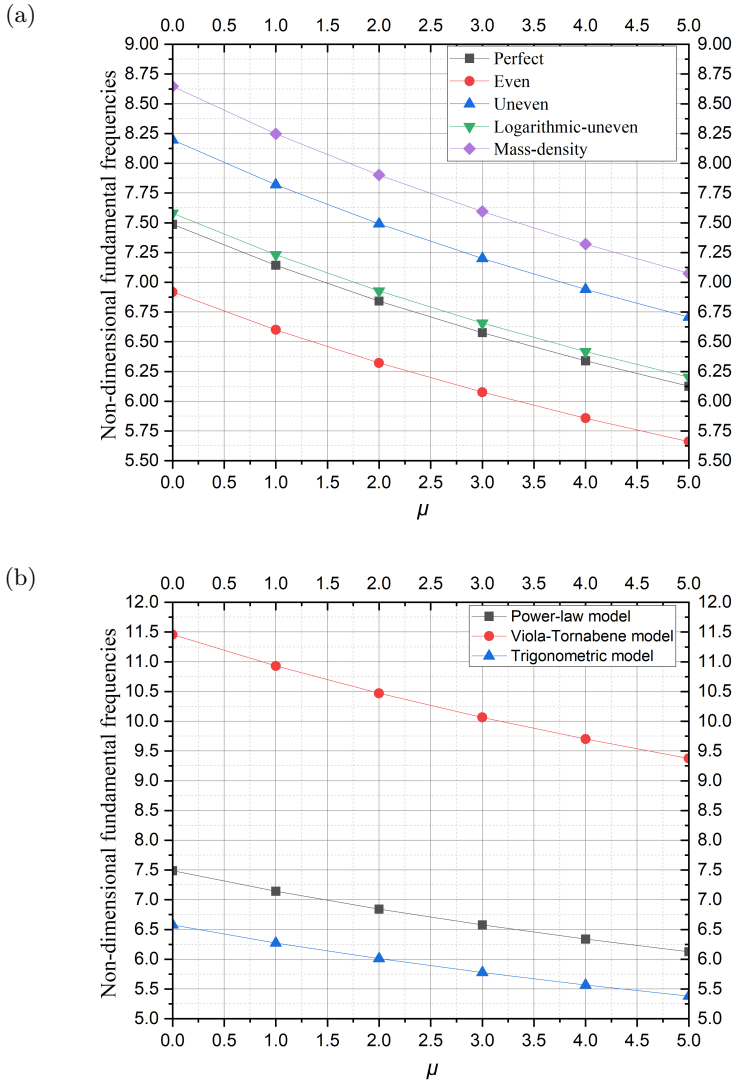


FIG. 3. Natural frequency variation of an FG nanobeam with nonlocal parameter ($P = 1$, $L/h = 10$).

the study explores different volume fraction models namely, the power-law, Viola–Tornabene four-parameter, and trigonometric models as illustrated in Fig. 3b. Throughout the analysis, the material index remains constant at 1, and the length-to-thickness ratio is set to 10.

The trends observed in Fig. 3 reveal that the natural frequency of FG nano-beams tends to decrease as the nonlocal parameter increases. This decrease in

frequency is attributed to the nonlocal parameter rendering the beam stiffer, thereby reducing its natural frequency. As the nonlocal parameter increases, the beam becomes increasingly rigid, leading to lower natural frequencies.

Upon closer examination of the various porosity models, it is evident that different distributions yield distinct natural frequency responses. Mass-density porosity consistently results in the highest non-dimensional fundamental frequency values, indicating that a denser material configuration enhances the beam's stiffness and consequently its natural frequency. Conversely, even porosity consistently yields the lowest natural frequency estimates, suggesting that a uniform distribution of pores leads to reduced natural frequencies (Fig. 3a).

Regarding the volume fraction models, the Viola–Tornabene four-parameter profile consistently yields the highest values for non-dimensional fundamental frequencies (ω), followed by the power-law model. The trigonometric model, on the other hand, exhibits the lowest deflection (Fig. 3b).

In summary, the observed decrease in natural frequency with increasing non-local parameter underscores its role in stiffening the beam, thereby reducing its dynamic response.

7.3. Effect of the material index of the FG nanobeam on its natural frequency

Figure 4 provides a comprehensive investigation into the influence of the material index on the natural frequency of FG porous nanobeams, covering a range from 0 to 30. This analysis encompasses various porosity and volume fraction models, representing diverse distributions such as uniform, non-uniform, logarithmic non-uniform, and mass-density-based distributions, as illustrated in Fig. 4a. Additionally, the study examines different volume fraction models, including the power-law, Viola–Tornabene four-parameter, and trigonometric models, as depicted in Fig. 4b. Throughout the analysis, the material index is systematically varied while maintaining a constant length-to-thickness ratio of 10, and the nonlocal parameter is set to 4.

As illustrated in both Fig. 4a and Fig. 4b, the natural frequency of the FG nanobeams decreases with an increase in the material index. This trend implies that higher material indices contribute to stiffer nanobeams, consequently leading to a reduction in their natural frequencies. Regarding the porosity models depicted in Fig. 4a, consistent patterns emerge. Mass-density porosity consistently yields the highest non-dimensional fundamental frequency values, indicating that denser material configurations enhance stiffness and subsequently decrease natural frequencies. Conversely, even porosity consistently yields the lowest natural frequency estimates, suggesting that a uniform distribution of pores results in a diminished dynamic response.

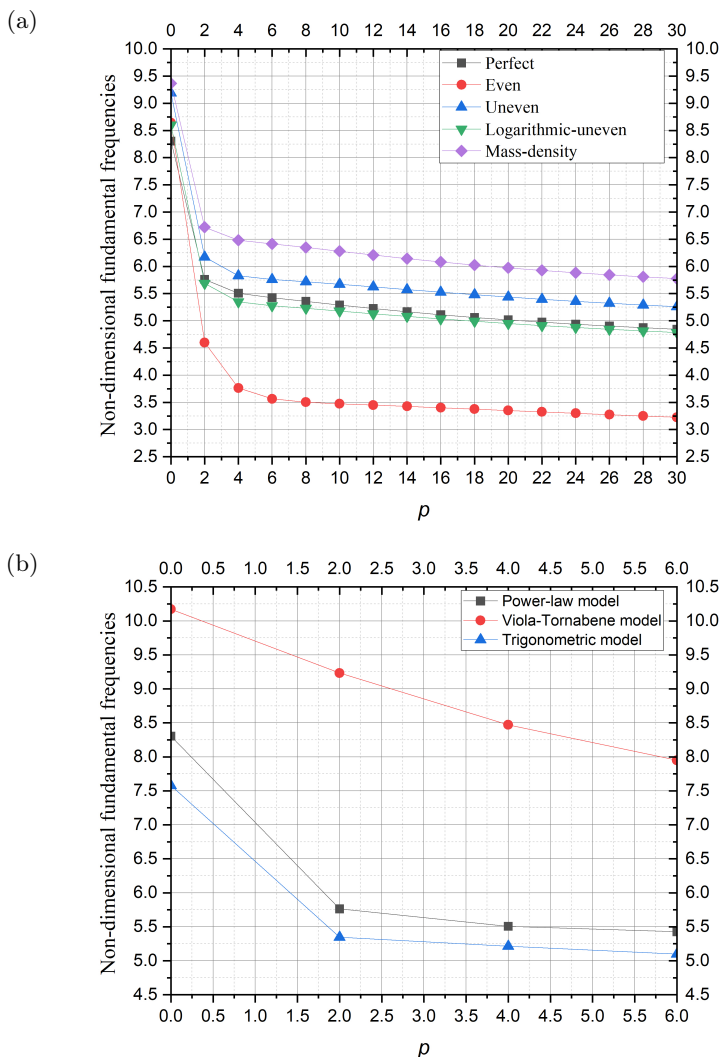


FIG. 4. Variation of the natural frequency of an FG nanobeam with material index ($\mu = 4$, $L/h = 10$).

Similarly, in the context of volume fraction models illustrated in Fig. 4b, the natural frequency decreases with an increasing material index, highlighting the stiffening effect of higher material indices on the nanobeams. Among the volume fraction models, the Viola–Tornabene four-parameter profile consistently yields the highest values for non-dimensional fundamental frequencies, followed by the power-law model. Conversely, the trigonometric model exhibits the lowest deflection.

These findings underscore the notable influence of the material index on the natural frequency behavior of FG nanobeams, emphasizing its crucial role in structural design and analysis.

7.4. Effect of types and porous coefficient ξ on the non-dimensional fundamental frequencies

Figure 5 delves into the dynamic behavior of FG nano-beams under the influence of different porosity types and the porous coefficient (ξ), as demonstrated in

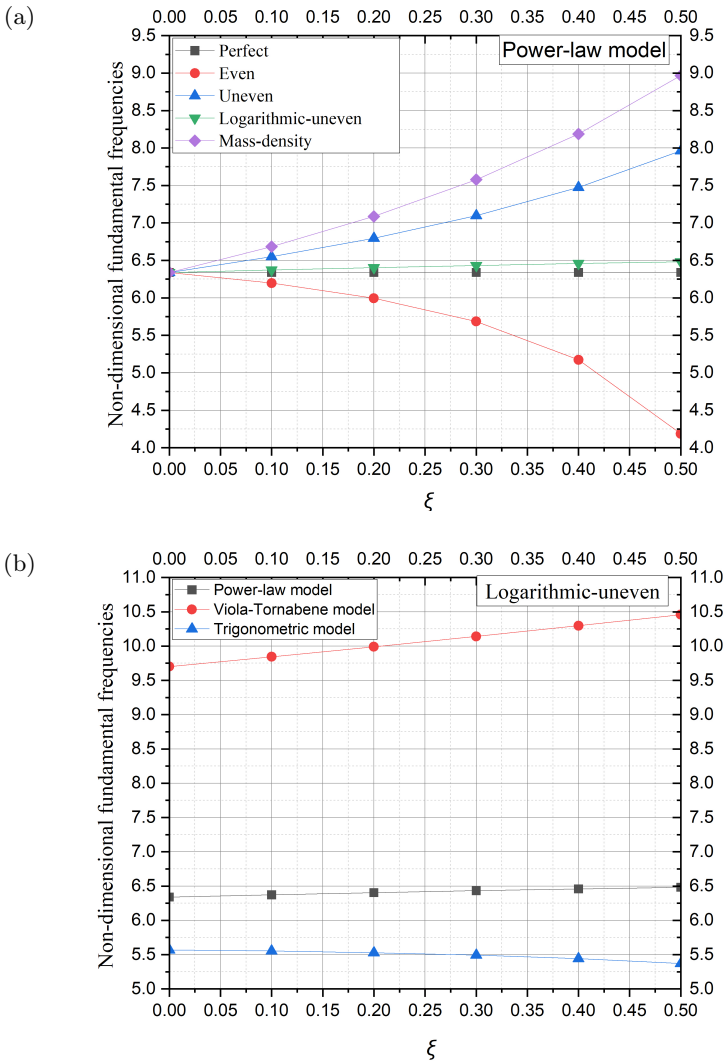


FIG. 5. Effect of types and porous coefficient ξ on the non-dimensional fundamental frequencies ($\mu = 4, L/h = 10$).

Fig. 5a. This investigation explores four distinct patterns of porosity variations: even porosity, uneven porosity, logarithmic-uneven porosity, and mass-density porosity. Additionally, various volume fraction models, such as the power-law, Viola–Tornabene four-parameter, and trigonometric models, depicted in Fig. 5b, are utilized to analyze the vibration characteristics while varying the porous coefficient (ξ).

The analysis involves adjusting the porous coefficient ξ from 0 to 0.5 in increments of 0.05, while maintaining a fixed gradient index ($P = 1$) and the thickness-to-span ratio ($a/h = 10$). Throughout these investigations, the nonlocal parameter remains constant at 4.

Figure 5a shows cases of the varied impact of different porosity profiles on the non-dimensional fundamental frequencies of FG nano-beams. Notably, the mass-density porosity profile consistently yields the highest frequencies, followed by uneven porosity, while even porosity exhibits the lowest values.

When the porous coefficient ξ increases, significant frequency enhancements are observed for the mass-density porosity profile, with uneven porosity showing a similar trend. However, logarithmic-uneven porosity experiences a slight increase, while even porosity sees a minor decrease in frequencies.

The dominance of the mass-density porosity model in yielding higher frequencies can be attributed to its consideration of true and apparent mass densities, which accurately capture the distribution of mass within the porous material. Moreover, increasing ξ amplifies the difference between true and apparent densities, resulting in higher frequencies. Conversely, the uniform distribution of pores in the even porosity model reduces stiffness and mass density, leading to lower frequencies. The uneven porosity model predicts higher frequencies due to non-uniform porosity concentration near the mid-plane, reducing effective mass density. Lastly, the gradual logarithmic variation of porosity in the logarithmic-uneven model introduces smoother changes in material properties, resulting in intermediate frequencies compared to even and uneven models.

In Fig. 5b, concerning volume fraction models, natural frequencies decrease with as the material index increases. The Viola–Tornabene four-parameter profile consistently yields the highest frequencies, followed by the power-law model. Conversely, the trigonometric model exhibits the lowest frequencies, suggesting a less effective distribution of material constituents in generating stiffness and mass density.

To gain a deeper understanding of the interplay between the nonlocal parameter (μ) and the porosity coefficient (ξ) on the fundamental frequency of an FG nanobeam, a 3D plot is presented in Fig. 6. This plot visualizes the relationship between these three variables, providing a comprehensive overview of their combined effect on the system's dynamic behavior.

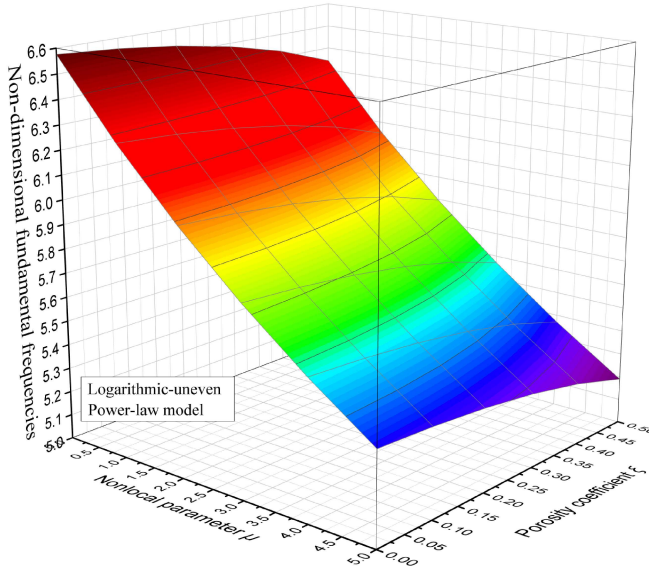


FIG. 6. 3D Visualization of natural frequency variation in an FG nanobeam with nonlocal parameter and porosity coefficient ($P = 1$, $L/h = 10$).

Figure 6 depicts a 3D plot where the x -axis represents the nonlocal parameter (μ), the y -axis represents the porosity coefficient (ξ), and the z -axis represents the fundamental frequency of the FG nanobeam. The plot is generated for specific conditions, namely $p = 1$ and $L/h = 10$, allowing for a focused analysis of the relationship between μ , ξ , and the fundamental frequency.

In Fig. 6, the 3D plot visually demonstrates how changes in the nonlocal parameter (μ) and the porosity coefficient (ξ) influence the fundamental frequency of the FG nanobeam. As the nonlocal parameter (μ) increases, there is a general decrease in the fundamental frequency, indicating that stronger nonlocal effects lead to a softer response of the system and subsequently lower natural frequencies. Likewise, for a fixed μ value, an increase in the porosity coefficient (ξ) results in a decrease in the fundamental frequency, reflecting the reduced stiffness of a more porous material, which allows for easier vibration at lower frequencies. This graphical representation underscores the intricate relationship between μ and ξ in shaping the dynamic behavior of FG nanobeams, offering valuable insights into their overall response.

We have performed a variance-based uncertainty analysis to assess the impact of uncertain input parameters on natural frequencies. Results show that the porosity coefficient (ξ) and the material index (p) contribute the most, accounting for 60% and 25% of the total variance, respectively. The nonlocal parameter (μ) and the length-to-thickness ratio (L/h) have smaller effects,

with variances of 10% and 5%. This analysis underscores the need for precise characterization of material properties and porosity distribution in FG porous nanobeam modeling.

8. Conclusions

This study establishes a comprehensive theoretical framework for analyzing the free vibration behavior of functionally graded (FG) porous nanobeams using the high-order shear deformation theory (HOSDT) and Eringen's nonlocal elasticity. The key novel contributions of this work are as follows:

1. **Integration of Advanced Porosity Models:** unlike previous studies that often focus on a single porosity distribution, this work incorporates four distinct porosity models uniform, non-uniform, logarithmic non-uniform, and mass-density-based to accurately capture the effects of porosity on the dynamic response of FG nanobeams. This approach provides a more comprehensive understanding of how porosity distribution influences natural frequencies and stiffness.
2. **The use of High-Order Shear Deformation Theory (HOSDT):** the application of HOSDT allows for a more accurate representation of shear deformation and rotary inertia, which are critical for thick nanobeams. This represents a significant improvement over classical beam theories, which often neglect these effects.
3. **Comprehensive Parametric Study:** a detailed parametric investigation was conducted to elucidate the influence of key factors, including the nonlocal parameter, the material index, the length-to-thickness ratio, and the porosity coefficient, on the natural frequencies of FG porous nanobeams. This study provides new insights into the interplay between material heterogeneity, porosity, and small-scale effects, offering valuable guidance for the design and optimization of these structures.
4. **Theoretical and Practical Implications:** the findings of this study have significant implications for the design of FG porous nanobeams in applications such as nanoelectromechanical systems (NEMS), energy harvesting devices, and biomedical sensors. The framework developed in this work can be extended to include additional effects, such as thermal or electromagnetic loads, and more complex geometries in future research.

In summary, this work advances the state-of-the-art in the dynamic analysis of FG porous nanobeams by integrating advanced modeling techniques, providing new physical insights, and offering a robust framework for future studies. The

results underscore the importance of considering material gradation, porosity distribution, and small-scale effects in the design and analysis of nanostructures.

Acknowledgments

The authors (Hafed and Zenkour) would like to express their gratitude to the Deanship of Research and Graduate Studies at King Khalid University for funding this work through Large Research Project under grant number RGP2/80/45.

References

1. S. RAI, A. GUPTA, *A novel dynamic stiffness matrix for the nonlocal vibration characteristics of porous functionally graded nanoplates on elastic foundation with small-scale effects*, The Journal of Strain Analysis for Engineering Design, 2024, <https://doi.org/10.1177/03093247241252199>.
2. W. XIAO, S. LIU, X. HUANG, X. WU, X. YUAN, *Vibration analysis of porous functionally graded material truncated conical shells in axial motion*, Mechanics, **30**, 2, 123–134, 2024, <https://doi.org/10.5755/j02.mech.34592>.
3. N.T. PHUONG, V.M. DUC, L.N. QUANG, *Nonlinear dynamic buckling analysis of the FG-GPLRC cylindrical and sinusoid panels with porous core under time-dependent axial compression*, Journal of Science and Transport Technology, **4**, 1, 13–22, 2024, <https://doi.org/10.58845/jstt.utt.2024.en.4.1.13-22>.
4. V. VAKA, P. SATHUJODA, N.A. BHALLA, S.V. YELIKE, *Finite element based dynamic analysis of a porous exponentially graded shaft system subjected to thermal gradients*, International Journal of Turbo & Jet-Engines, in press, 2025, <https://doi.org/10.1515/tjj-2023-0103>.
5. V.S. CHANDEL, M. TALHA, *The random thermo-elastic nonlinear vibration analysis of porous FGM nano-beams using the first order perturbation theory*, Proceedings of the Institution of Mechanical Engineers, Part C: Journal of Mechanical Engineering Science, **238**, 11, 5241–5257, 2024, <https://doi.org/10.1177/09544062231212>.
6. L. KURPA, T. SHMATKO, J. AWREJCWICZ, G. TIMCHENKO, I. MORACHKOVSKA, *Analysis of free vibration of porous power-law and sigmoid functionally graded sandwich plates by the R-functions method*, Journal of Applied and Computational Mechanics, **9**, 4, 1144–1155, 2023, <https://doi.org/10.22055/jacm.2023.43435.4082>.
7. P. ZHANG, P. SCHIAVONE, H. QING, *Dynamic stability analysis of porous functionally graded beams under hygro-thermal loading using nonlocal strain gradient integral model*, Applied Mathematics and Mechanics, **44**, 12, 2071–2092, 2023, <https://doi.org/10.1007/s10483-023-3059-9>.
8. M. ZANJANCHI NIKOO, M. LEZGI, S. SABOURI GHOMI, M. GHADIRI, *Dynamic instability analysis of timoshenko FG sandwich nanobeams subjected to parametric excitation*, Proceedings of the Institution of Mechanical Engineers, Part C: Journal of Mechanical Engineering Science, **238**, 7, 2891–2905, 2024, <https://doi.org/10.1177/09544062231196632>.

9. M.A. ATTIA, R.A. SHANAB, *Dynamic analysis of 2DFGM porous nanobeams under moving load with surface stress and microstructure effects using Ritz method*, Acta Mechanica, **235**, 1, 1–27, 2024, <https://doi.org/10.1007/s00707-023-03703-2>.
10. M. ZANJANCHI, M. GHADIRI, S. SABOURI-GHOMI, *Dynamic stability and bifurcation point analysis of FG porous core sandwich plate reinforced with graphene platelet*, Acta Mechanica, **234**, 10, 5015–5037, 2023, <https://doi.org/10.1007/s00707-023-03638-8>.
11. G. LI, Z. YAN, *Application of a semi-analytical method to the dynamic analysis of functionally graded porous conical–conical–cylindrical shell*, AIP Advances, **13**, 6, 2023, <https://doi.org/10.1063/5.0152397>.
12. M. AKHZARY, A.R. KHORSHIDVAND, *A mixed DQ-Newmark method for dynamic response and stress analysis of porous FG rectangular plates under moving load*, Special Topics & Reviews in Porous Media: An International Journal, **14**, 6, 2023, <https://doi.org/10.1615/SpecialTopicsRevPorousMedia.v14.i6.30>.
13. N.T. GIANG, T.T.T. THUY, N.T.H. VAN, *A novel finite element model in nonlocal transient analysis of viscoelastic functionally graded porous nanoplates resting on viscoelastic medium*, Mathematical Methods in the Applied Sciences, **47**, 4, 2076–2098, 2024, <https://doi.org/10.1002/mma.9735>.
14. M. TAŞKIN, Ö. DEMİR, *Effect of porosity distribution on vibration and damping behavior of inhomogeneous curved sandwich beams with fractional derivative viscoelastic core*, Engineering Computations, **40**, 3, 538–563, 2023, <https://doi.org/10.1108/EC-04-2022-0269>.
15. J. LU, Q. YANG, Z. MENG, K. YANG, W. XU, C.V. CHIU, *Modeling and dynamic analysis of functionally graded porous spherical shell based on Chebyshev–Ritz approach*, Science and Engineering of Composite Materials, **30**, 1, 20220214, 2023, <https://doi.org/10.1515/secm-2022-0214>.
16. Y. BERKIA, A. REBAI, B. LITOUCHE, S. ABBAS, K. MANSOURI, *Investigating parametric homogenization models for natural frequency of FGM nano beams*, AIMS Materials Science, **10**, 5, 2023, <https://doi.org/10.3934/mat.2023048>.
17. K. FOROUTAN, L. DAI, *Non-linear hygrothermal analysis of imperfect multilayer functionally graded shallow shell with a porous core*, Journal of the Brazilian Society of Mechanical Sciences and Engineering, **45**, 3, 151, 2023, <https://doi.org/10.1007/s40430-023-04026-y>.
18. R. BILLEL, *Effect of the idealization models and thermal loads on deflection behavior of sandwich FGM plate*, International Conference on Electrical Engineering and Photonics (EExPolytech), 260–264, IEEE, 2022, <https://doi.org/10.1109/EExPolytech56308.2022.9950823>.
19. B. REBAI, K. MANSOURI, M. CHITOUR, A. BERKIA, T. MESSAS, F. KHADRAOUI, B. LITOUCHE, *Effect of idealization models on deflection of functionally graded material (FGM) plate*, Journal of Nano- and Electronic Physics, **15**, 1, 01022, 2023, [https://doi.org/10.21272/jnep.15\(1\).01022](https://doi.org/10.21272/jnep.15(1).01022).
20. X. SHEN, T. LI, L. XU, F. KIARASI, M. BABAEI, K. ASEMI, *Free vibration analysis of FG porous spherical cap reinforced by graphene platelet resting on Winkler foundation*, Advances in Nano Research, **16**, 1, 11–26, 2024, <https://doi.org/10.12989/anr.2024.16.1.011>.
21. B. UZUN, Ö. CIVALEK, M. YAYLIB, *Size dependent torsional vibration of a rotationally restrained circular FG nanorod via strain gradient nonlocal elasticity*, Advances in Nano Research, **16**, 2, 175–186, 2024, <https://doi.org/10.12989/anr.2024.16.2.175>.

22. E. MADENCI, Ş. GÜLCÜ, K. DRAICHE, *Analytical nonlocal elasticity solution and ANN approximate for free vibration response of layered carbon nanotube reinforced composite beams*, *Advances in Nano Research*, **16**, 3, 251–263, 2024, <https://doi.org/10.12989/anr.2024.16.3.251>.
23. Y. TANG, H. QING, *Static bending study of AFG nanobeam using local stress-and strain-driven nonlocal integral models*, *Advances in Nano Research*, **16**, 3, 265–272, 2024, <https://doi.org/10.12989/anr.2024.16.3.265>.
24. E. ZARE, D.K. VORONKOVA, O. FARAJI, H. AGHAJANIREFAH, H.M. NIA, M. GHOLAMI, M.G. AZANDARIANI, *Assessment of nonlocal nonlinear free vibration of bi-directional functionally-graded Timoshenko nanobeams*, *Advances in Nano Research*, **16**, 5, 473–487, 2024, <https://doi.org/10.12989/anr.2024.16.5.473>.
25. E.E. GHANDOURAH, A.A. DAIKH, S. KHATIR, A.M. ALHAWSAWI, E.M. BANOQITAH, M.A. ELTAHER, *A dynamic analysis of porous coated functionally graded nanoshells rested on viscoelastic medium*, *Mathematics*, **11**, 10, 2407, 2023, <https://doi.org/10.3390/math11102407>.
26. C. LI, L. YAO, W. CHEN, S. LI, *Comments on nonlocal effects in nano-cantilever beams*, *International Journal of Engineering Science*, **87**, 47–57, 2015, <https://doi.org/10.1016/j.ijengsci.2014.11.006>.
27. J. FERNÁNDEZ-SÁEZ, R. ZAERA, *Vibrations of Bernoulli-Euler beams using the two-phase nonlocal elasticity theory*, *International Journal of Engineering Science*, **119**, 232–248, 2017, <https://doi.org/10.1016/j.ijengsci.2017.06.021>.
28. G. ROMANO, R. BARRETTA, M. DIACO, F.M. DE SCIARRA, *Constitutive boundary conditions and paradoxes in nonlocal elastic nanobeams*, *International Journal of Mechanical Sciences*, **121**, 151–156, 2017, <https://doi.org/10.1016/j.ijmecsci.2016.10.036>.
29. A.M. ZENKOUR, A.F. RADWAN, *A compressive study for porous FG curved nanobeam under various boundary conditions via a nonlocal strain gradient theory*, *The European Physical Journal Plus*, **136**, 248, 2021, <https://doi.org/10.1140/epjp/s13360-021-01238-w>.
30. M.A. ABAZID, A.M. ZENKOUR, M. SOBHY, *Wave propagation in FG porous GPLs-reinforced nanoplates under in-plane mechanical load and Lorentz magnetic force via a new quasi 3D plate theory*, *Mechanics Based Design of Structures and Machines*, **50**, 5, 1831–1850, 2022, <https://doi.org/10.1080/15397734.2020.1769651>.
31. A.M. ZENKOUR, R.A. ALGHANMI, *A refined quasi-3D theory for the bending of functionally graded porous sandwich plates resting on elastic foundations*, *Thin-Walled Structures*, **181**, 110047, 2022, <https://doi.org/10.1016/j.tws.2022.110047>.
32. A. FOROOGHI, S. REZAEY, S.M. HAGHIGHI, A.M. ZENKOUR, *Thermal instability analysis of nanoscale FG porous plates embedded on Kerr foundation coupled with fluid flow*, *Engineering with Computers*, **38**, 4, 2953–2973, 2022, <https://doi.org/10.1007/s00366-021-01426-3>.
33. R.M. TANTAWY, A.M. ZENKOUR, *Rotating exponentially graded variable-thickness annular piezoelectric porous disks*, *Journal of Vibration Engineering & Technologies*, **13**, 166, 1–14, 2025, <https://doi.org/10.1007/s42417-024-01676-7>.
34. Q-H. PHAM, H.T. NHAN, V.K. TRAN, A.M. ZENKOUR, *Hygro-thermo-mechanical vibration analysis of functionally graded porous curved nanobeams resting on elastic foundations*, *Waves in Random and Complex Media*, in press, 2025, <https://doi.org/10.1080/17455030.2023.2177500>.

-
35. P. ZHANG, H. QING, C.F. GAO, *Exact solutions for bending of Timoshenko curved nanobeams made of functionally graded materials based on stress-driven nonlocal integral model*, *Composite Structures*, **245**, 112362, 2020, <https://doi.org/10.1016/j.compstruct.2020.112362>.
 36. E. SAMANIEGO, C. ANITESCU, S. GOSWAMI, V.M. NGUYEN-THANH, H. GUO, K. HAMDIA, X. ZHUANG, T. RABCZUK, *An energy approach to the solution of partial differential equations in computational mechanics via machine learning: concepts, implementation and applications*, *Computer Methods in Applied Mechanics and Engineering*, **362**, 112790, 2020, <https://doi.org/10.1016/j.cma.2019.112790>.
 37. X. ZHUANG, H. GUO, N. ALAJLAN, H. ZHU, T. RABCZUK, *Deep autoencoder based energy method for the bending, vibration, and buckling analysis of Kirchhoff plates with transfer learning*, *European Journal of Mechanics-A/Solids*, **87**, 104225, 2021, <https://doi.org/10.1016/j.euromechsol.2021.104225>.
 38. T. RABCZUK, H. REN, X. ZHUANG, *A nonlocal operator method for partial differential equations with application to electromagnetic waveguide problem*, *Computers, Materials & Continua*, **59**, 1, 31–55, 2019, <https://doi.org/10.15488/4766>.
 39. H. REN, X. ZHUANG, T. RABCZUK, *A nonlocal operator method for solving partial differential equations*, *Computer Methods in Applied Mechanics and Engineering*, **358**, 112621, 2020, <https://doi.org/10.1016/j.cma.2019.112621>.

Received October 19, 2024; revised version February 13, 2025.

Published online April 7, 2025.
